Journal of Advanced Research 24 (2020) 69–78

Contents lists available at ScienceDirect

Journal of Advanced Research

journal homepage: www.elsevier.com/locate/jare

Whole-cell fungal-mediated structural transformation of anabolic drug metenolone acetate into potent anti-inflammatory metabolites

Mahwish Siddiqui [a], Atia-tul-Wahab [b,*], Almas Jabeen [b], Yan Wang [a], Wei Wang [c], Atta-ur-Rahman [a], M. Iqbal Choudhary [a,b,d,*]

[a] H. E. J. Research Institute of Chemistry, International Center for Chemical and Biological Sciences, University of Karachi, Karachi 75270, Pakistan
[b] Dr. Panjwani Center for Molecular Medicine and Drug Research, International Center for Chemical and Biological Sciences, University of Karachi, Karachi 75270, Pakistan
[c] School of Pharmacy, Hunan University of Chinese Medicine, Changsha, Hunan 410208, People's Republic of China
[d] Department of Chemistry, Faculty of Science and Technology, Universitas Airlangga, Komplek Campus C, Surabaya 60115, Indonesia

GRAPHICAL ABSTRACT

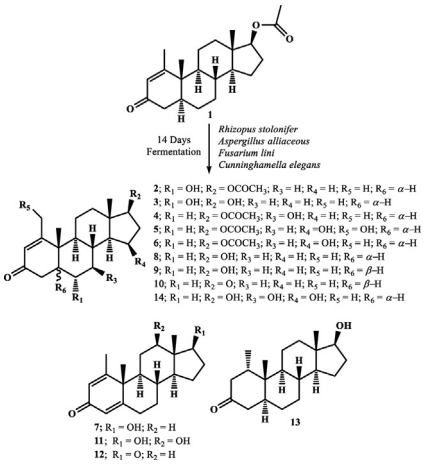

ARTICLE INFO

Article history:
Received 20 December 2019
Revised 8 February 2020
Accepted 12 February 2020
Available online 15 February 2020

Keywords:
Microbial transformation
Anabolic drug
Matenolone acetate
Anti-inflammatory

ABSTRACT

Seven new derivatives, 6α-hydroxy-1-methyl-3-oxo-5α-androst-1-en-17-yl acetate (**2**), 6α,17β-dihydroxy-1-methyl-3-oxo-5α-androst-1-en (**3**), 7β-hydroxy-1-methyl-3-oxo-5α-androst-1-en-17-yl acetate (**4**), 15β,20-dihydroxy-1-methyl-3-oxo-5α-androst-1-en-17-yl acetate (**5**), 15β-hydroxy-1-methyl-3-oxo-5α-androst-1-en-17-yl acetate (**6**), 12β,17β-dihydroxy-1-methyl-3-oxoandrosta-1,4-dien (**11**), and 7β,15β,17β-trihydroxy-1-methyl-3-oxo-5α-androst-1-en (**14**), along with six known metabolites, 17β-hydroxy-1-methyl-3-oxoandrosta-1,4-dien (**7**), 17β-hydroxy-1-methyl-3-oxo-5α-androst-1-en (**8**), 17β-hydroxy-1-methyl-3-oxo-5β-androst-1-en (**9**), 1-methyl-5β-androst-1-en-3,17-dione (10), 1-methyl-3-oxoandrosta-1,4-dien-3,17-dione (**12**), and 17β-hydroxy-1α-methyl-5α-androstan-3-one (**13**) of metenolone acetate (**1**), were synthesized through whole-cell biocatalysis with *Rhizopus stolonifer*, *Aspergillus alliaceous*, *Fusarium lini*, and *Cunninghamella elegans*. Atamestane (**12**), an aromatase inhibitor, was synthesized for the first time *via F. lini*-mediated transformation of **1** as the major product.

Peer review under responsibility of Cairo University.

* Corresponding authors at: Dr. Panjwani Center for Molecular Medicine and Drug Research, International Center for Chemical and Biological Sciences, University of Karachi, Karachi 75270, Pakistan (Atia-tul-Wahab); H. E. J. Research Institute of Chemistry, International Center for Chemical and Biological Sciences, University of Karachi, Karachi 75270, Pakistan (M.I. Choudhary).
E-mail addresses: atia.tulwahab@iccs.edu (Atia-tul-Wahab), iqbal.choudhary@iccs.edu (M.I. Choudhary).

https://doi.org/10.1016/j.jare.2020.02.009
2090-1232/

Hydroxylation, dehydrogenation, and reduction were occurred during biocatalysis. Study indicated that *F. lini* was able to catalyze dehydrogenation reactions selectively. Structures of compounds **1**–**14** were determined through NMR, HRFAB-MS, and IR spectroscopic data. Compounds **1**–**14** were identified as non-cytotoxic against BJ human fibroblast cell line (ATCC CRL-2522). Metabolite **5** (81.0 ± 2.5%) showed a potent activity against TNF-α production, as compared to the substrate **1** (62.5 ± 4.4%). Metabolites **2** (73.4 ± 0.6%), **8** (69.7 ± 1.4%), **10** (73.2 ± 0.3%), **11** (60.1 ± 3.3%), and **12** (71.0 ± 7.2%), also showed a good inhibition of TNF-α production. Compounds **3** (IC_{50} = 4.4 ± 0.01 μg/mL), and **5** (IC_{50} = 10.2 ± 0.01 μg/mL) showed a significant activity against T-cell proliferation. Identification of selective inhibitors of TNF-α production, and T-cell proliferation is a step forward towards the development of anti-inflammatory drugs.

Introduction

Steroids form an important class of biologically active natural or semi-synthetic organic compounds. Several steroidal-based, antiaromatase, anticancer, antiinflammatory, antileishmanial, antimicrobial, antiandrogenic, anabolic, and contraceptive drugs have been developed over the past few decades. Besides their benefits, existing steroidal drugs are also associated with various adverse effects, including gynecomastia and reduced fertility in males, masculinization in females and children, blood clotting, hypertension, atherosclerosis, hepatic neoplasms, jaundice, and carcinoma, *etc*. [1–4].

Metenolone acetate (**1**) ($C_{22}H_{32}O_3$) is a synthetic steroidal anabolic drug, previously sold under the brands, Primobolan, and Nibal for the treatment of anemia. The drug is also used by athletes, and for sports animals to enhance their muscular strength and physical performances. As compared to the 17α-alkylated anabolic steroidal drugs, metenolone acetate (**1**), and metenolone enanthate are preferred, as they have higher anabolic efficiencies with lower androgenic, and hepatotoxic effects [5–8].

Currently a significant number of steroidal drugs have been structurally modified either through chemical syntheses or by biotransformation in order to improve their pharmacodynamic profiles, and safety. Generally, conventional chemical derivatizations involve protection, deprotection, and functional group activation steps through the use of toxic, hazardous, and expensive reagents and catalysts under extreme reaction conditions, resulting in high E-factors (increased production of wastes, as compared to the desired products). According to the green processes, reducing E-factors is of particular interest for pharmaceutical industries. In contrast, microbial transformation is an effective approach, as microorganisms have smaller size, efficient multiplication, high surface-volume ratio, and higher metabolic and growth rates, yielding a range of enzymes in a short duration. This leads to the synthesis of chemo-, enantio-, regio-, and stereo-selective/specific derivatives. Moreover, microbial biotransformation techniques involve the use of non-toxic, low cost, and eco-friendly biological catalysts (whole colonies of microbes) at ambient temperature, pressure, and pH, catalyzing oxidation, reduction, dehydrogenation, chlorination, aromatization, methylation, *etc*., and reducing the total number of steps towards the desired products [9–14].

Microbes, *e.g*., bacteria, fungi, yeasts, *etc*. due to the presence of bio-catalytic hemeproteins, also known as CYPs (cytochrome P450), are successfully used for the selective/specific hydroxylation at sp^3 hybridized carbon atoms and aromatic rings, epoxidation at C=C atoms, dehydrogenation, reduction, and aromatization of inert organic molecules [14–16].

Inflammation is an effort of host for self-protections, after the introduction of pathogens, such as bacteria, virus, fungi, or any irritant in the body, activating the process of healing. Most of the cancers arise from the long-term irritations, infections, and inflammations, suggesting a connection between inflammation, and cancers. Thus chronic inflammation is a serious risk factor towards the onset of cancers. Glucocorticoids (GCs), and other steroid-based compounds are among the most effective anti-inflammatory agents [17–19].

In continuation of our fungal-mediated biotransformation studies on steroidal drugs [8,20–29], and in search of new anti-inflammatory agents, metenolone acetate (**1**) was subjected to the biotransformation with *Rhizopus stolonifer* (Fig. 1), *Aspergillus alliaceous* (Fig. 1), *Fusarium lini* (Fig. 2), and *Cunninghamella elegans* (Fig. 2). This afforded thirteen metabolites **2**–**14**. Among them, metabolites **2**–**6**, **11**, and **14** were identified as new. Compound **1**, and its metabolites **2**–**14** were assessed for their inhibition potential against cytokine (TNF-α) production, and T-cell proliferation.

Materials and methods

Fungal cell cultures and media

A. alliaceous (ATCC 10060), *R. stolonifer* (TSY 047), *C. elegans* (ATCC 36114), and *F. lini* (NRRL 2204) were used for fungal-assisted structural modifications of an anabolic-androgenic steroidal drug, metenolone acetate (**1**).

Media ingredients (1 L) for the growth of microorganisms were as follows:

5 g NaCl, 5 g potassium dihydrogen phosphate, 5 g peptone, 10 g Glucose, 10 mL glycerol, and 1 L dist. water.

General experimental

Metenolone acetate (**1**), (m/z = 344.2, $C_{22}H_{32}O_3$), was procured from the Shenzhen Simeiquan Biotechnology Company Limited, China. Media constituents were acquired from VWR Chemicals (UK), Oxoid Limited (UK), Sigma-Aldrich (Germany), Scharlau Chemicals & Reagents (Spain), and Dae-Jung Chemicals & Metals Company Limited (Korea). Number of compounds, along with their purity, were determined on silica-coated (PF_{254}) TLCs. Silica gel (70–230 mesh) column chromatography was performed for the fractionation of gummy crude materials. Fractions were fully-purified *via* recycling reverse phase HPLC (LC–908, YMC L-80) using acetonitrile/water. 1D, and 2D NMR of compounds **1**–**14** were performed in deuterated-chloroform on the Bruker Avance-NMR (Bruker, Switzerland). FAB-, and HRFAB-MS were done on the mass spectrometer, Joel JMS H × 110 (Joel, Japan). Absorbances for compounds **2**–**14** in the UV spectrum were noted on spectrophotometer, Evolution 300 UV–visible (Hitachi, Japan). Optical rotations (JASCO P–2000 polarimeter, JASCO, Japan), and melting points (Buchi 560 device, Buchi, Switzerland) were performed for compounds **2**–**14**. Bruker Vector 22 spectrophotometer (Bruker, France) was used for IR data of metabolites.

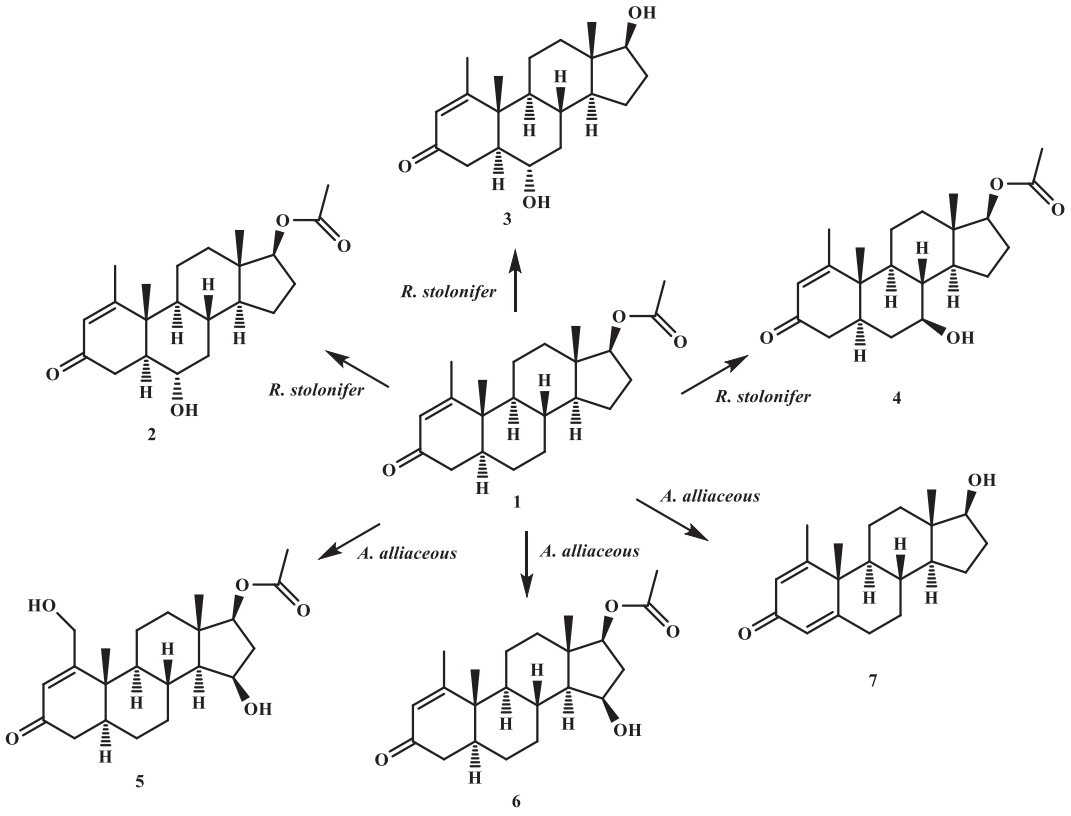

Fig. 1. Biotransformation of metenolone acetate (**1**) with *Rhizopus stolonifer* TSY 047, and *Aspergillus alliaceous* ATCC 10060.

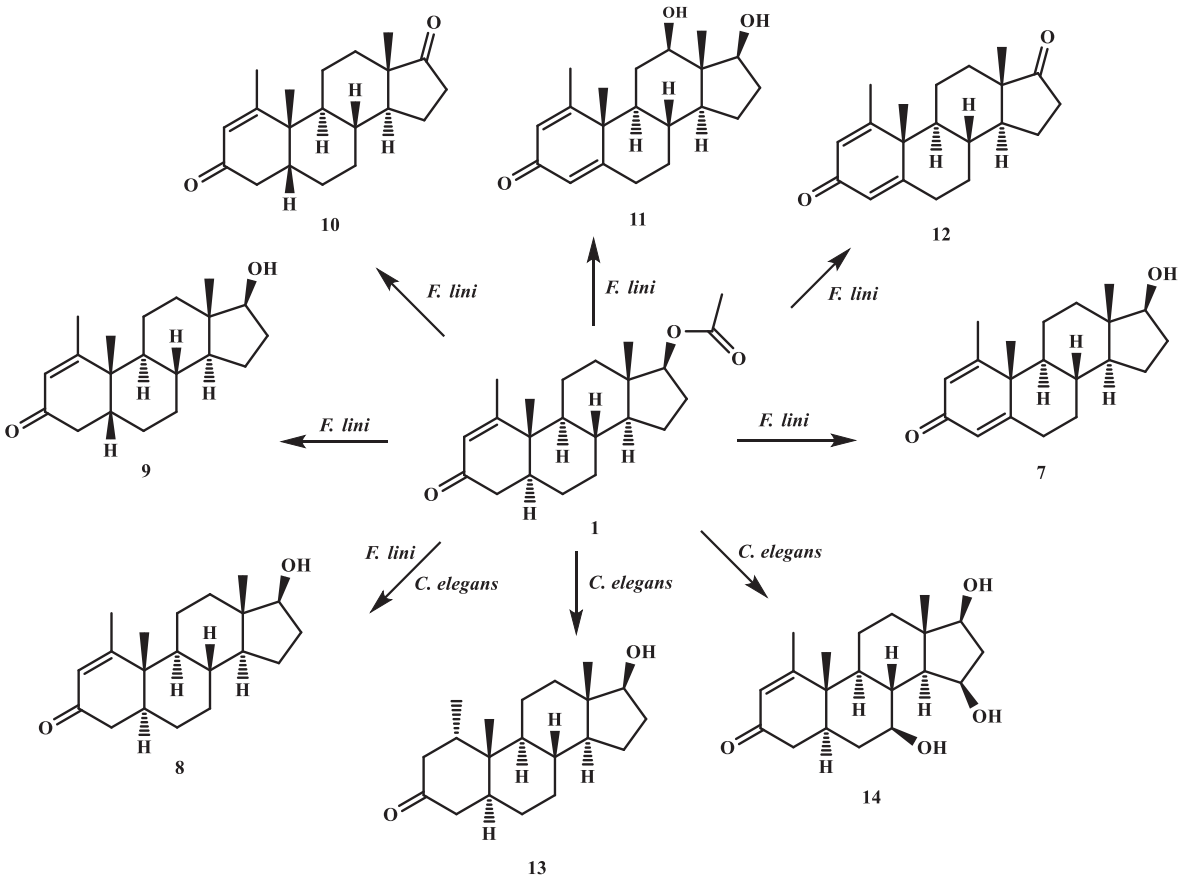

Fig. 2. Biotransformation of metenolone acetate (**1**) with *Fusarium lini* NRRL 2204, and *Cunninghamella elegans* ATCC 36114.

*Fermentation of metenolone acetate **(1)***

Fungal-mediated biotransformation of **1** was performed in two scales, e.g., small, and large. In small scale, media (0.4 L) was prepared, added 0.1 L to four Erlenmeyer flasks of 0.25 L (four flasks for each fungus), cotton plugged, autoclaved, and cooled at room temperature. Among them, two flasks were served as test flasks (for the incubation period of 7 and 14 days), while remaining two flasks were prepared as positive (media + drug), and negative (media + fungus) controls. After mature, and maximum growth of each fungus, drug **1** (15 mg) was mixed in 1 mL of acetone, dispensed in each fungal-containing test flasks, and placed on a shaker. Flasks were harvested after 7th and 14th days. The flasks were extracted with EtOAc. Sodium sulfate was added into the extracts to make them moisture free, and concentrated by using rotary evaporator. This yielded gummy crude materials. Number of transformations in each crude were analyzed and compared with positive and negative controls on silica gel TLC plates, followed by staining with ceric sulfate or phosphomolybdic acid spraying reagents. On the basis of experimental scale results, compound **1** was proceeded for the preparative scale biotransformation experiments by using *R. stolonifer* (2 g of compound **1** in 12 L media), *A. alliaceous* (2 g of compound **1** in 12 L media), *F. lini* (3 g of compound **1** in 16 L media), and *C. elegans* (2 g of compound **1** in 12 L media) in order to obtain the transformed products.

Extraction and isolation protocol

Concentrated crude extracts (A-D), obtained from the preparative scale experiments, were fractionated through silica gel CC. Hexanes-acetone solvent systems were used as a mobile phase for each crude material. The polarity was changed as 5–100% gradient of polar solvent (acetone), passing 0.4 L at each concentration, which yielded a total of fifteen main fractions. The fractions were analyzed by silica gel TLCs. Fractions (1–3) were obtained from the crude A (3.95 g). Metabolites **2** (Water-CH_3CN, 3/7; R_T = 21 min; 11.3211 mg), **3** (Water-CH_3CN, 3/7; R_T = 19 min; 9.9121 mg), and **4** (Water-CH_3CN, 3/7; R_T = 22 min; 5.3121 mg) were purified *via* recycling RP- HPLC from fractions 1–3, respectively. Fractions (4–6) were obtained from the crude B (4.14 g). Compounds **5** (Water-CH_3CN, 3/7; R_T = 31 min; 4.1265 mg), **6** (Water-CH_3CN, 3/7; R_T = 29 min; 8.9812 mg), and **7** (Water-CH_3CN, 3/7; R_T = 33 min; 26.3141 mg) were purified *via* recycling RP- HPLC from fractions 4–6, respectively. Fractions (7–12) were obtained from the crude C (7.42 g). Metabolites **8** (Water-CH_3CN, 4/6; R_T = 31 min; 71.2121 mg), **9** (Water-CH_3CN, 4/6; R_T = 27 min; 8.4221 mg), **10** (Water-CH_3CN, 4/6; R_T = 29 min; 3.1211 mg), **11** (Water-CH_3CN, 4/6; R_T = 23 min; 7.2125 mg), **12** (Water-CH_3CN, 4/6; R_T = 34 min; 244.8923 mg), and **7 (**2.4214 mg) were purified *via* recycling RP- HPLC from fractions 7–12, respectively. Fractions (13–15) were obtained from the crude D (3.78 g). Compounds **13** (Water-CH_3CN, 3/7; R_T = 22 min; 4.5112 mg), **14** (Water-CH_3CN, 3/7, R_T = 37 min; 5.4814 mg), and **8** (61.3475 mg) were purified *via* recycling RP- HPLC from fractions 10–12, respectively.

*6α-Hydroxy-1-methyl-3-oxo-5α-androst-1-en-17-yl acetate **(2)***

White solid; UV λ_{max} (log ε): 230 (5.69); melting point: 154–157 °C;$[\alpha]_D^{25}$= +76.6 (*c* 0.0008); HRFAB-MS (+ve mode) *m/z* 361.2355 $[M+H]^+$ (calc. 361.2379) ($C_{22}H_{33}O_4$); FAB-MS (+ve mode) *m/z* 361.2 $[M+H]^+$; IR υ_{max} (cm^{-1}): 3408 (OH), 2931 (CH), 1729 (O—C=O), 1661 and 1596 (C=C—C=O); ^{1}H NMR data: Table 1; ^{13}C NMR data: Table 2.

*6α-17β-Dihydroxy-1-methyl-3-oxo-5α-androst-1-en **(3)***

White solid; UV λ_{max} (log ε): 243 (6.08); melting point: 191–194 °C;$[\alpha]_D^{25}$= +63.5 (*c* 0.0014); HRFAB-MS (+ve mode) *m/z* 319.2281 $[M+H]^+$ (calc. 319.2273) ($C_{20}H_{31}O_3$); FAB-MS (+ve mode) *m/z* 319.3 $[M+H]^+$; IR υ_{max} (cm^{-1}): 3411 (OH), 2943 (CH), 1658 and 1597 (C=C—C=O); ^{1}H NMR data: Table 1; ^{13}C NMR data: Table 2.

*7β-Hydroxy-1-methyl-3-oxo-5α-androst-1-en-17-yl acetate **(4)***

White solid; UV λ_{max} (log ε): 243 (6.32); melting point: 153–156 °C;$[\alpha]_D^{25}$= +108.1 (*c* 0.0012); HRFAB-MS (+ve mode) *m/z* 361.2368 $[M+H]^+$ ($C_{22}H_{33}O_4$, calc. 361.2379); FAB-MS (+ve mode) *m/z* 361.1 $[M+H]^+$; IR υ_{max} (cm^{-1}): 3433 (OH), 2928 (CH), 1728 (O-C=O), 1663 and 1597 (C=C—C=O); ^{1}H NMR data: Table 1; ^{13}C NMR data: Table 2.

*15β,20-Dihydroxy-1-methyl-3-oxo-5α-androst-1-en-17-yl acetate **(5)***

White solid; UV λ_{max} (log ε): 230 (7.6); melting point: 211–214 °C;$[\alpha]_D^{25}$= +127.0 (*c* 0.0008); HRFAB-MS (+ve mode) *m/z* 377.2346 $[M+H]^+$ (calc. 377.2328) ($C_{22}H_{33}O_5$); FAB-MS (+ve mode) *m/z* 377.1 $[M+H]^+$; IR υ_{max} (cm^{-1}): 3431 (OH), 2935 (CH), 1725 (O-C=O), 1662 and 1595 (C=C—C=O); ^{1}H NMR data: Table 1; ^{13}C NMR data: Table 2.

*15β-Hydroxy-1-methyl-3-oxo-5α-androst-1-en-17-yl acetate **(6)***

White solid; UV λ_{max} (log ε): 243 (7.05); melting point: 171–173 °C;$[\alpha]_D^{25}$= +46.1 (*c* 0.0028); HRFAB-MS (+ve mode) *m/z* 361.2371 $[M+H]^+$ (calc. 361.2379) ($C_{22}H_{33}O_4$); FAB-MS (+ve mode) *m/z* 361.3 $[M+H]^+$; IR υ_{max} (cm^{-1}): 3421 (OH), 2924 (CH), 1730 (O—C=O), 1658 and 1597 (C=C—C=O); ^{1}H NMR data: Table 1; ^{13}C NMR data: Table 2.

*17β-Hydroxy-1-methyl-3-oxoandrosta-1,4-dien **(7)***

White solid; UV λ_{max} (log ε): 248 (6.50); melting point: 204–206 °C;$[\alpha]_D^{25}$= −158.1 (*c* 0.0024); HRFAB-MS (+ve mode) *m/z* 301.2178 $[M+H]^+$ (calc. 301.2168) ($C_{20}H_{29}O_2$); FAB-MS (+ve mode) *m/z* 301.1 $[M+H]^+$; IR υ_{max} (cm^{-1}): 3410 (OH), 2945 (CH), 1657 and 1610 (C=C—C=O).

*17β-Hydroxy-1-methyl-3-oxo-5α-androst-1-en **(8)***

White solid; UV λ_{max} (log ε): 243 (6.2); melting point: 159–163 °C;$[\alpha]_D^{25}$= −105.7 (*c* 0.0014); HRFAB-MS (+ve mode) *m/z* 303.2314 $[M+H]^+$ (calc. 303.2324) ($C_{20}H_{31}O_2$); FAB-MS (+ve mode) *m/z* 303.2 $[M+H]^+$; IR υ_{max} (cm^{-1}): 3433 (OH), 2934 (CH), 1662 and 1595 (C=C—C=O).

*17β-Hydroxy-1-methyl-3-oxo-5β-androst-1-en **(9)***

White solid; UV λ_{max} (log ε): 243 (6.4); melting point: 208–210 °C;$[\alpha]_D^{25}$= +58.4 (*c* 0.0015); HRFAB-MS (+ve mode) *m/z* 303.2315 $[M+H]^+$ (calc. 303.2324) ($C_{20}H_{31}O_2$); FAB-MS (+ve mode) *m/z* 303.2 $[M+H]^+$; IR υ_{max} (cm^{-1}): 3411 (OH), 2930 (CH), 1659 and 1604 (C=C—C=O).

*1-Methyl-5β-androst-1-en-3,17-dione **(10)***

White solid; UV λ_{max} (log ε): 231 (6.8); melting point: 199–202 °C;$[\alpha]_D^{25}$= +58.4 (*c* 0.0022); HRFAB-MS (+ve mode) *m/z* 301.2175 $[M+H]^+$ (calc. 301.2168) ($C_{20}H_{29}O_2$); FAB-MS (+ve mode)

m/z 303.2 $[M+H]^+$; IR υ_{max} (cm^{-1}): 2933 (CH), 1736 (C=O), 1663 and 1603 (C=C—C=O).

12β,17β-Dihydroxy-1-methyl-3-oxoandrosta-1,4-dien ***(11)***

White solid; UV λ_{max} (log ε): 248 (7.9); melting point: 203–205 °C;$[\alpha]_D^{25}$= +77.1 (*c* 0.0009); HRFAB-MS (+ve mode) *m/z* 317.2111 $[M+H]^+$ (calc. 317.2117) ($C_{20}H_{29}O_3$); FAB-MS (+ve mode) *m/z* 317.2 $[M+H]^+$; IR υ_{max} (cm^{-1}): 3412 (OH), 2949 (CH), 1656 and 1605 (C=C—C=O); ^{1}H NMR data: Table 2; ^{13}C NMR data: Table 2.

1-Methyl-3-oxoandrosta-1,4-dien-3,17-dione ***(12)***

White solid; UV λ_{max} (log ε): 248 (6.9); melting point: 163–166 °C;$[\alpha]_D^{25}$= +78.6 (*c* 0.0015); HRFAB-MS (+ve mode) *m/z* 299.2022 $[M+H]^+$ (calc. 299.2011) ($C_{20}H_{27}O_2$); FAB-MS (+ve mode) *m/z* 299.1 $[M+H]^+$; IR υ_{max} (cm^{-1}) 2940 (CH), 1737 (C=O), 1659 and 1618 (C=C—C=O).

17β-Hydroxy-1α-methyl-5α-androstan-3-one ***(13)***

White solid; UV λ_{max} (log ε): 212 (3.82); melting point: 172–174 °C;$[\alpha]_D^{25}$= −70.4 (*c* 0.0021); HRFAB-MS (+ve mode) *m/z* 305.2491 $[M+H]^+$ (calc. 305.2481) ($C_{20}H_{33}O_2$); FAB-MS (+ve mode) *m/z* 305.2 $[M+H]^+$; IR υ_{max} (cm^{-1}): 3413 (OH), 2934 (CH), and 1708 (C=O).

7β,15β,17β-Trihydroxy-1-3-oxo-5α-androst-1-en ***(14)***

White solid; UV λ_{max} (log ε): 242 (5.8); melting point: 233–236 °C;$[\alpha]_D^{25}$= +54.5 (*c* 0.0031); HRFAB-MS (+ve mode) *m/z* 335.2211 $[M+H]^+$ (calc. 335.2222) ($C_{20}H_{31}O_4$); FAB-MS (+ve mode) *m/z* 335.1 $[M+H]^+$; IR υ_{max} (cm^{-1}): 3378 (OH), 2926 (CH), 1663 and 1594 (C=C—C=O); ^{1}H NMR data: Table 1; ^{13}C NMR data: Table 2.

Cytokine inhibition assay

The inhibition potential of compounds **1**–**14** against cytokine (TNF-α) production in human leukemia cell line (THP-1) was evaluated by applying the reported protocol [30]. In this assay, THP-1 cell line from the ECCC (UK) were grown, and maintained in the RPMI-1640, comprising mercaptoethanol (50 μM), sodium pyruvate (1 mM), FBS (10%), glucose (5.5 mM), L-glutamine (2 mM), and HEPES (10 mM). At confluency of 70%, 2.5×10^5 cells/mL were plated in 24- well plates of cell culture. PMA (phorbol myristate acetate) (20 ng/mL) was added to differentiate them into the macrophage mimicking cells, and incubated for 24 h in the presence of 5% CO_2 at 37 °C. Lipopolysaccharide B of *Escherichia coli* (50 ng/mL) was used to stimulate the culture, assessed with compounds **1**–**14**, and placed for 240 min in 5% CO_2 at 37 °C. TNF-α level in the supernatants was determined on ELISA through human Duo Set kit (R & D Systems) (USA), according to instructions of manufacturer.

T-cells proliferation assay

The inhibition potential of test compounds against T-cell proliferation *in vitro* was determined by using the reported procedure [31]. In this assay, T-lymphocytes were obtained from heparinized blood of healthy human, and mixed 10 mL of blood with RPMI-1640 (10 mL). Resulting mixture was gently layered on LSM (5 mL), and tubes were centrifuged for 20 min at 400 g at 25 °C. The collected buffy layer was then supplemented with RPMI-1640, and centrifuged for 600 s at 4 °C. Pellet having PBMCs was mixed with RPMI (1 mL), comprising FBS (5%). Proliferation of T-cells was determined by applying Alamar Blue assay. PMBCs (2×10^6 cells/mL) were added in a 96- well plates. T-lymphocytes were activated with phytohemagglutinin-L (7.5 μg/mL). Test compounds with different concentrations in triplicates were added to it, and plates were placed for 2 days at 37 °C in 5% CO_2. Alamar Blue dye (a one-tenth volume) was added into it, and reincubated for 4 h. Absorbances were recorded at wavelengths of 570, and 600 nm in a spectrophotometer.

Results and discussion

Fermentation of metenolone acetate (**1**) (*m/z* 344.2, $C_{22}H_{32}O_3$) with *R. stolonifer*, *A. alliaceous*, *F. lini*, and *C. elegans* yielded seven new, and six known derivatives.

Metabolite **2** presented the $[M^+]$ in the HRFAB-MS (+ve mode) at *m/z* 361.2355 ($C_{22}H_{33}O_4$, calc. 361.2379), suggesting hydroxylation of compound **1** (*m/z* 344.2, $C_{22}H_{32}O_3$). Absorbances (cm^{-1}) at 1596 and 1661 (C=C—C=O), 1729 (O—C=O), and 3408 (OH) were noted in the IR spectrum. NMR chemical shifts data (Tables 1 and 2) of metabolite **2** were distinctly comparable to the drug **1**. Additional downfield signals in the ^{1}H- (δ 3.50, td), and the ^{13}C- (δ 69.1) NMR spectra were observed, indicating hydroxylation of **1**. OH group at C-6 (δ 69.1), was inferred *via* the key HMBC interactions (Fig. 3) of δ 2.84, dd (H_2-4), δ 1.79, overlap (H-5) and δ 1.92, dt (H_2-7) with δ 69.1 (C-6), and δ 3.50, td (H-6) with δ 35.9 (C-4), δ 51.0 (C-5) and δ 35.5 (C-8). Likewise, δ 3.50, td (H-6) showed key COSY correlations with δ 1.79, overlap (H-5) and δ 1.92, dt; 0.94, q (H_2-7) (Fig. 3). Equatorial-orientation of an OH group at C-6 (δ 69.1) was determined *via* the Key NOESY interactions of *axially*-oriented H-6 (δ 3.50, td) with β-oriented protons, *i.e.*, H-8 (δ 1.52, overlap), and CH_3-19 (δ 1.04, s) (Fig. 4). The structure was deduced as 6α-hydroxy metenolone acetate (**2**).

The HRFAB-MS (+ve) of **3** presented the $[M^+]$ at *m/z* 319.2281 ($C_{20}H_{31}O_3$, calc. 319.2273), suggesting the hydrolysis of ester moiety and hydroxylation of **1** (*m/z* 344.2, $C_{22}H_{32}O_3$). Absorbances (cm^{-1}) at 1597 and 1658 (C=C—C=O), and 3411 (OH), were noted in the IR spectrum. NMR chemical shifts data (Tables 1 and 2) of metabolite **3** were distinctly similar to the compounds **1** and **2**. Signals for acetate at C-17, and methylene at C-6 were not appeared in the ^{1}H NMR spectrum, and the ^{13}C NMR spectrum of transformed product **3**. Similar to the metabolite **2**, new downfield signals in the ^{1}H- (δ 3.50, td) and ^{13}C- (δ 69.1) NMR spectra were observed. The hydroxyl at C-6 (δ 69.1) was deduced *via* the key HMBC interactions (Fig. 3) of δ 2.32, dd (H-4), δ 1.80, overlap (H-5), and δ 1.92, dt (H_2-7) with δ 69.1 (C-6), and δ 3.50, td (H-6) with δ 35.9 (C-4), and δ 51.2 (C-5). The key COSY interactions (Fig. 3) of δ 3.50, td (H-6) with δ 1.80, overlap (H-5), and δ 1.92, dt; 0.94, q (H_2-7) also supported hydroxylation at C-6. Equatorial-orientation of hydroxyl at C-6 was deduced *via* NOESY interactions (Fig. 4) of *axially*-oriented H-6 (δ 3.50, td) with β-oriented protons, *i.e.*, H-8 (δ 1.52, overlap), and CH_3-19 (δ 1.05, s). The structure of **3** was determined as 6α-hydroxy metenolone.

Compound **4** presented the $[M^+]$ in the HRFAB-MS (+ve) at *m/z* 361.2368 ($C_{22}H_{33}O_4$, calc. 361.2379), suggesting the hydroxylation of substrate **1** (*m/z* 344.2, $C_{22}H_{32}O_3$). IR showed absorbances at 3433 (hydroxyl), 1728 (ester), and 1663 and 1597 (α, β-CO) cm^{-1}. NMR chemical shifts data of **4** (Tables 1 and 2) were distinctly similar to the **1**, and **2**. New deshielded signals at δ 3.40, and 72.6 were noted in the ^{1}H, and ^{13}C NMR spectra of **4**. Signals for methylene protons (H_2-7), and methylene carbon (C-7) were also not appeared in the NMR spectra of **4**. An OH at C-7 (δ 72.6) was placed based on the key HMBC interactions (Fig. 3) of δ 1.66, dt (H_2-6), and δ 1.47, overlap (H-8) with δ 72.6 (C-7), and the key COSY interactions (Fig. 3) of δ 3.40, m (H-7) with δ 1.66, dt; 1.44, overlap (H_2-6), and δ 1.47, overlap (H-8). Equatorial-orientation

Table 1
^{1}H NMR chemical shifts (J in Hz) of new compounds **2**–**6**, **11**, and **14** in $CDCl_3$.

Carbons	**2**	**3**	**4**	**5**	**6**	**11**	**14**
1	–	–	–	–	–	–	–
2	5.73, s	5.73, s	5.71, s	6.17, s	5.70, s	6.17, s	5.73, s
3	–	–	–	–	–	–	–
4	2.84, dd ($J_{4,4}$ = 18.5; $J_{4,5}$ = 4.2); 2.31, dd ($J_{4,4}$ = 18.5; $J_{4,5}$ = 13.2)	2.83, dd ($J_{4,4}$ = 18.4; $J_{4,5}$ = 3.8); 2.32, dd ($J_{4,4}$ = 18.5; $J_{4,5}$ = 13.2)	2.38, dd ($J_{4,4}$ = 18.3; $J_{4,5}$ = 13.5); 2.20, dd ($J_{4,4}$ = 18.3; $J_{4,5}$ = 4.2)	2.41, dd ($J_{4,4}$ = 18.4; $J_{4,5}$ = 13.6); 2.24, dd ($J_{4,4}$ = 18.4; $J_{4,5}$ = 3.6)	2.37, dd ($J_{4,4}$ = 18.3; $J_{4,5}$ = 13.6); 2.20, dd ($J_{4,4}$ = 18.3; $J_{4,5}$ = 3.8)	6.06, s	2.40, dd ($J_{4,4}$ = 18.3; $J_{4,5}$ = 13.5); 2.21, dd ($J_{4,4}$ = 18.3; $J_{4,5}$ = 3.8)
5	1.79, overlap	1.80, overlap	1.99, m	1.99, overlap	1.96, overlap	–	2.01, m
6	3.50, td ($J_{a,a}$ = 10.8; $J_{a,e}$ = 4.0)	3.50 td ($J_{a,a}$ = 10.8; $J_{a,e}$ = 4.0)	1.66, dt ($J_{a,a}$ = 11.8; $J_{a,e}$ = 3.9); 1.44, overlap	1.44 2[H], overlap	1.46 2[H], overlap	2.61, td ($J_{a,a}$ = 12.8; $J_{a,e}$ = 5.4); 2.36, ddd ($J_{a,e}$ = 6.9; $J_{a,e}$ = 4.8; $J_{6,4}$ = 2.0)	1.65, overlap; 1.58, overlap
7	1.92, dt ($J_{a,a}$ = 12.0; $J_{a,e}$ = 3.8); 0.94, q (J = 12.2)	1.92, dt ($J_{a,a}$ = 12.0; $J_{a,e}$ = 3.8); 0.94, q (J = 12.1)	3.40, m	1.95, overlap; 1.01, overlap	1.94, overlap; 1.03, overlap	1.72, m; 0.95, m	3.57, overlap
8	1.52, overlap	1.52, overlap	1.47, overlap	1.81, ddd ($J_{a,a}$ = 14.1; $J_{a,a}$ = 11.7; $J_{a,e}$ = 3.6)	1.82, overlap	1.70, overlap	1.84, m
9	1.18, overlap	1.18, overlap	1.28, overlap	1.23, overlap	1.22, overlap	1.13, m	1.30, m
10	–	–	–	–	–	–	–
11	1.65, m; 1.35, m	1.62, m; 1.33, m	1.46, overlap; 1.27, overlap	1.71, overlap; 1.49, overlap	1.49, overlap; 1.24, overlap	1.79, 2[H], overlap	2.12, overlap; 1.54, overlap
12	1.72, overlap; 1.27, m	1.79, overlap; 1.17, overlap	1.74, dt ($J_{\alpha,\alpha}$ = 12.8; $J_{\alpha,e}$ = 3.0); 1.28, m	1.72, overlap; 1.22, overlap	1.72, overlap; 1.23, overlap	3.43, dd ($J_{a,a}$ = 10.6; $J_{a,e}$ = 4.9)	1.78, overlap; 1.13, overlap
13	–	–	–	–	–	–	–
14	1.22, overlap	1.15, overlap	1.37, m	1.01, overlap	1.03, overlap	0.81, m	1.02, m
15	1.42 2[H], overlap	1.47 2[H], overlap	1.80 2[H], overlap	4.22, m	4.22, m	1.63, m; 1.43, overlap	4.28, m
16	2.15, m; 1.50, overlap	2.07, m; 1.44, overlap	2.16, overlap; 1.52, overlap	2.68, ddd ($J_{16,16}$ = 14.8; $J_{16,17}$ = 8.8; $J_{16,15}$ = 7.5); 1.61, ddd ($J_{16,16}$ = 14.7; $J_{16,17}$ = 8.1; $J_{16,15}$ = 1.9)	2.68, ddd ($J_{16,16}$ = 14.8; $J_{16,17}$ = 8.8; $J_{16,15}$ = 7.5); 1.63, ddd ($J_{16,16}$ = 14.8; $J_{16,17}$ = 8.1; $J_{16,15}$ = 2.0)	2.06, overlap; 1.48, overlap	2.57, ddd ($J_{16,16}$ = 14.5; $J_{16,17}$ = 8.1; $J_{16,15}$ = 8.6); 1.63, overlap
17	4.63, t ($J_{17,16}$ = 8.0)	3.67, t ($J_{17,16}$ = 8.4)	4.60, t ($J_{17,16}$ = 8.5)	4.51 t ($J_{17,16}$ = 8.5)	4.52 t ($J_{17,16}$ = 8.5)	3.82, t ($J_{17,16}$ = 8.6)	3.57, overlap
18	0.83, s	0.79, s	0.87, s	1.10, s	1.07, s	0.85, s	1.09, s
19	1.04, s	1.05, s	1.05, s	1.11, s	1.11, s	1.32, s	1.12, s
20	2.06, s	2.06, s	2.06, s	4.46, dd ($J_{20,20}$ = 16.3; $J_{20,2}$ = 1.3); 4.37, dd ($J_{20,20}$ = 16.2; $J_{20,2}$ = 1.0)	2.05, d ($J_{20,2}$ = 1.0)	2.12, d ($J_{20,2}$ = 0.9)	2.07, s
21	–		–	–	–		
22	2.03, s		2.03, s	2.04, s	2.04, s		

Table 2
^{13}C NMR chemical shifts of new compounds **2**–**6**, **11**, and **14**.

Carbons	**2**	**3**	**4**	**5**	**6**	**11**	**14**
1	171.2	171.2	171.2	173.0	172.2	169.7	171.1
2	129.0	129.0	129.1	124.6	128.8	129.3	129.2
3	198.9	198.9	198.7	199.4	199.3	186.0	198.5
4	35.9	35.9	40.7	41.5	41.3	123.9	41.0
5	51.0	51.2	41.4	45.0	44.8	165.7	42.1
6	69.1	69.1	37.9	28.4	28.5	32.9	38.4
7	39.7	39.7	72.6	29.4	29.5	33.6	73.0
8	35.5	35.7	45.7	34.5	34.6	34.6	41.3
9	49.3	49.5	49.6	50.0	50.4	47.9	50.0
10	42.5	42.8	41.8	42.0	42.0	46.5	42.9
11	23.6	23.5	25.8	25.3	25.0	33.7	25.7
12	37.0	36.8	37.3	38.8	38.8	78.6	38.3
13	43.6	43.7	43.5	42.7	42.8	47.8	41.9
14	51.0	51.1	51.2	55.7	55.8	55.5	56.7
15	25.1	25.2	26.3	69.6	69.6	23.6	70.4
16	27.3	30.4	27.8	40.3	40.2	29.8	40.6
17	82.4	81.6	82.1	81.7	81.8	81.7	81.3
18	12.6	11.6	13.0	14.6	13.9	6.0	13.9
19	15.2	15.2	13.8	15.3	15.4	16.3	14.5
20	24.8	24.9	24.9	63.7	25.3	23.5	25.1
21	171.1		171.2	171.1	171.1		
22	21.1		21.1	21.0	21.1		

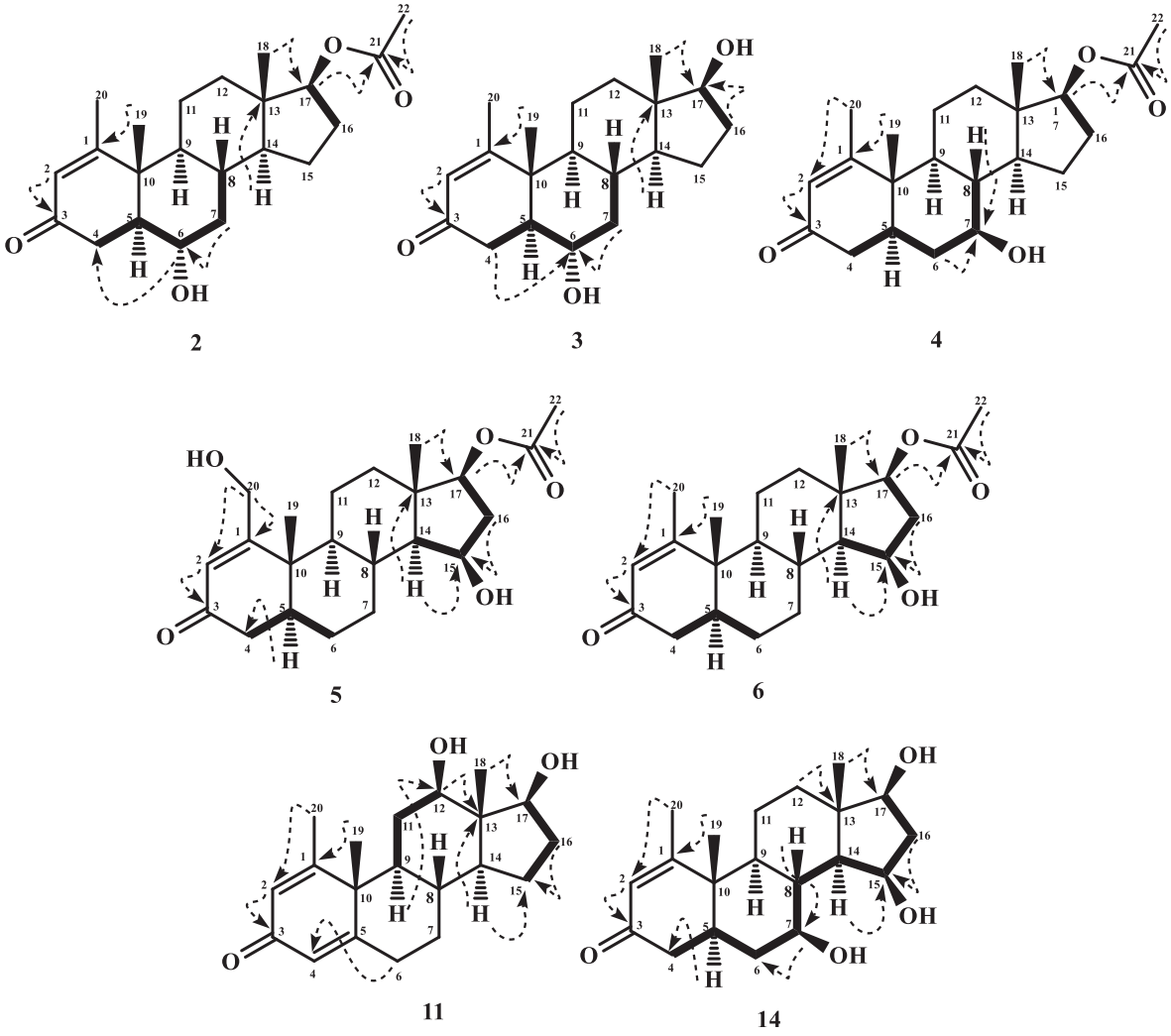

Fig. 3. Key HMBC (- - - - ➤), and COSY (▬) correlations in new compounds **2–6, 11** and **14**.

of hydroxyl at C-7 (δ 72.6) was inferred *via* the key NOESY correlations (Fig. 4) of *axially*-oriented H-7 (δ 3.40, m) with α-oriented protons, *i.e.*, H-5 (δ 1.99, m), H-9 (δ 1.28, overlap), and H-14 (δ 1.37, overlap). The structure of **4** was thus deduced as 7β-hydroxy metenolone acetate.

The HRFAB-MS (+ve) of **5** presented the [M^+] at *m/z* 377.2346 ($C_{22}H_{33}O_5$, calc. 377.2328), suggesting the dihydroxylation of drug **1** (*m/z* 344.2, $C_{22}H_{32}O_3$). IR showed absorbances at 3431 (hydroxyl), 1725 (ester), and 1662 and 1595 cm^{-1} (α, β-unsaturated carbonyl). NMR chemical shifts data (Tables 1 and 2) of **5** were distinctly similar to the **1**, **2** and **4**. The ^{1}H, and the ^{13}C NMR spectra showed new deshielded signals at δ 4.22 (m), 4.46, (dd), and 4.37 (dd), and δ 69.6, and 63.7, respectively. Signals for methylene and methyl protons, and methylene and methyl carbons were also not appeared in the NMR spectra of **5**. A hydroxyl group at C-15 (δ 69.6) was assigned *via* the key HMBC interactions (Fig. 3) of δ 1.66, ddd (H-16), and δ 1.01, overlap (H-14) with δ 69.6 (C-15), and δ 4.22, m (H-15) with δ 81.7 (C-17), δ 40.3 (C-16), and δ 42.7 (C-13). The COSY correlations (Fig. 3) of δ 4.22, m (H-15) with δ 2.68, ddd;1.66, ddd; 1.44, overlap (H_2-16) and δ 1.01, overlap (H-14) also supported the placement. β-Orientation of OH at C-15 (δ 69.6) was assigned through the key NOESY interaction (Fig. 4) of α-oriented H-14 (δ 31.01, overlap) with H-15 (δ 4.22, m). An OH at C-20 (δ 63.7) was placed *via* the key HMBC interactions (Fig. 3) of δ 6.17, s (H-2) with C-20, and δ 4.46, dd; 4.37, dd (H_2-20) with δ 173.0 (C-1), and δ 124.6 (C-2), and through the key COSY interactions (Fig. 3) of δ 6.17, s (H-2) with δ 4.46, dd; 4.37, dd (H_2-20). The structure of **5** was deduced as 15β,20-dihydroxy metenolone acetate.

Metabolite **6** exhibited the [M^+] in the HRFAB-MS (+ve) at *m/z* 361.2371 ($C_{22}H_{33}O_4$, calc. 361.2379), suggesting the hydroxylation of drug **1** (*m/z* 344.2, $C_{22}H_{32}O_3$). The IR showed absorbances at 3421 (hydroxyl), 1730 (ester), and 1658 and 1597 (α, β-unsaturated CO) cm^{-1}. NMR chemical shifts data (Tables 1 and 2) of metabolite **6** showed distinct similarities with the compounds **1**, and **5** NMR spectra. Downfield signal in the ^{1}H- (δ 4.22, m), and the ^{13}C- (δ 69.6) NMR spectra were observed, indicating the hydroxylation of compound **1**. Placement of a hydroxyl at C-15 (δ 69.1) was based on the key HMBC interactions (Fig. 3) of δ 4.22, m (H-15) with δ 81.8 (C-17), and δ 40.2 (C-16), and δ 1.63, ddd (H-16), and δ 1.03, overlap (H-14) with δ 69.1 (C-15). The key COSY correlations (Fig. 3) of δ 4.22, m (H-15) with δ 2.68, ddd; 1.63, ddd (H_2-16), and δ 1.03, overlap (H-14) also supported hydroxylation at C-15. β-Orientation of hydroxyl at C-15 was assigned *via* the key NOESY interactions (Fig. 4) of *axially*-oriented H-14 (δ 1.03, overlap)) with H-15 (δ 4.22, m). The structure of **6** was thus deduced as 15β-hydroxy metenolone acetate.

Compound **7** was identified as 17β-hydroxy-1-methylandrosta-1,4-dien-3-one by using NMR, HRFAB-MS, and IR spectral data. It was previously synthesized by Lourdusamy with his group through

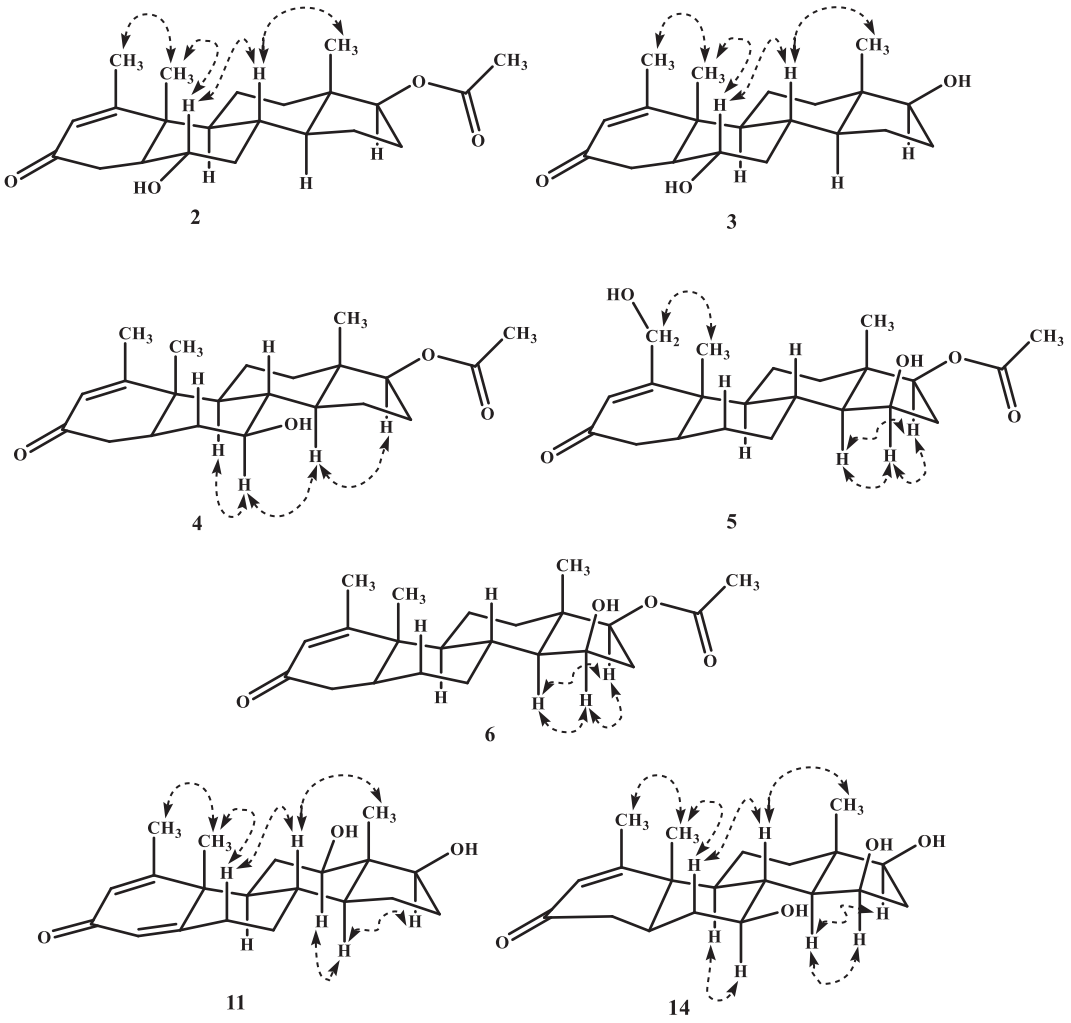

Fig. 4. Key NOESY (↔) correlations in new compounds **6**, **11,** and **14**.

dibromination, dehydrobromination, and hydrolysis of mesterolone acetate [32].

Compound **8** was identified as metenolone by analyzing its spectral data, previously reported by our research group *via A. niger*-assisted biotransformation of metenolone enanthate [8].

Metabolite **9** was deduced as 17β-hydroxy-1-methyl-3-oxo-5β-androst-1-en analyzing its spectral data. It was reported through metabolism of the steroidal aromatase inhibitor, atamestane (**12**) in monkeys, rats, and humans [33].

Metabolite **10** was deduced as 1-methyl-5β-androsta-3,17-dione-1-ene by studying its spectral data. The compound **10** was reported *via* metabolism of the steroidal aromatase inhibitor, atamestane (**12**) in monkeys, rats, and humans [33].

The HRFAB-MS (+ve mode) of **11** presented the [M^+] at *m*/*z* 317.2111 ($C_{20}H_{29}O_3$, calc. 317.2117), suggesting the dehydrogenation, hydroxylation, and hydrolysis of ester group in metenolone acetate (**1**) (*m*/*z* 344.2, $C_{22}H_{32}O_3$). The IR showed absorbances at 3412 (hydroxyl), and 1656 and 1605 (α, β-unsaturated CO) cm^{-1}. NMR chemical shifts data (Tables 1 and 2) **11** were distinctly similar to the **7**. The ^{1}H NMR spectrum displayed new deshielded signals for olefinic (δ 6.06, s), and oxymethine protons (δ 3.43, dd). Similarly, the ^{13}C NMR spectrum showed new deshielded signals for olefinic at δ 165.7, and 123.9, and oxymethine carbons at δ 78.6. Signals for CH_2-4 and CH_2-12 were not appeared in the NMR spectra of **11**. Dehydrogenation between C-5/C-4 was inferred *via* the key HMBC interactions (Fig. 3) of δ 6.06, s (H-4) with δ 129.3 (C-2), δ 46.5 (C-10), and δ 32.9 (C-6), δ 2.61, td; 2.36, ddd (H_2-6) with δ 123.9 (C-4), and δ 165.7 (C-5). The key COSY correlations (Fig. 3) (allylic coupling) of δ 6.06, s (H-4) with δ 2.61, td, 2.36, ddd (H_2-6) also supported the position. The OH at C-12 (δ 78.6) was placed based on the key HMBC interactions (Fig. 3) of δ 3.82, t (H-17), and δ 1.79, 2[H], overlap (H_2-11) with δ 78.6 (C-12), and δ 3.43, dd (H-12) with δ 81.7 (C-17), and δ 6.0 (C-18). The key COSY correlations (Fig. 3) of δ 3.43, dd (H-12) with δ 1.79, 2[H], overlap (H_2-11) also supported an OH at C-12. β-Orientation of OH at C-12 was inferred *via* the NOESY correlations (Fig. 4) of α-oriented H-12 (δ 3.43, dd) with *axially*-oriented protons, e.g., H-14 (δ 0.81, m), H-9 (δ 1.13, m), and H-17 (δ 3.82, t). The structure of **11** was deduced as 12β,17β-dihydroxy-1-methy landrosta-1,4-diene-3-one.

Atamestane (**12**), which is in clinical trials as anti-aromatase, was obtained for the first time through *F. lini*-mediated biotransformation of **1**. Compound **12** was previously synthesized by Lourdusamy *et al.* in 1995 using mesterolone acetate as the starting material [33].

Metabolites **13**, an anabolic steroid, was identified as mesterolone by using NMR, HRFAB-MS, IR spectral data [28].

Metabolite **14** showed the [M^+] in the HRFAB-MS (+ve mode) at *m*/*z* 335.2211 ($C_{20}H_{31}O_4$, calc. 335.2222), suggesting the hydrolysis of ester moiety, along with dihydroxylation of metenolone acetate (**1**) (*m*/*z* 344.2, $C_{22}H_{32}O_3$). The IR showed absorbances at 3378 (hydroxyl), and 1663 and 1594 (α, β-unsaturated CO) cm^{-1}. NMR

chemical shifts data (Tables 1 and 2) of **14** were similar to the **8**. The ^{1}H NMR spectrum displayed new deshielded signals for oxymethine protons at δ 3.57, overlap, and 4.28, m. Similarly, the ^{13}C NMR spectrum dishielded new oxymethines carbon signals at δ 73.0, and 70.4. Signals for methylene (CH_2-7, and CH_2-15), and acetate groups were not appeared in the NMR spectra of **14**. The first OH at C-7 (δ 73.0) was determined *via* the key HMBC interactions (Fig. 3) of δ 3.57, overlap (H-7) with δ 38.4 (C-6), and δ 56.7 (C-14), and δ 1.65, overlap;1.58, overlap (H_2-6), and δ 1.84, m (H-8) with C-7, and through the COSY interactions (Fig. 3) of δ 3.57, overlap (H-7) with δ 1.65, overlap;1.58, overlap (H_2-6), and δ 1.84, m (H-8). β-Orientation of hydroxyl at C-7 was deduced *via* the NOESY correlations (Fig. 4) of α-oriented H-7 (δ 3.57, overlap) with *axially*-oriented protons, *i.e.*, H-5 (δ 2.01, m), and H-14 (δ 1.02, m). Hydroxylation at C-15 (δ 70.4) was deduced through the key HMBC interactions (Fig. 3) of δ 4.28, m (H-15) with δ 81.3 (C-17), and δ 40.6 (C-16), and δ 1.63, overlap (H-16) with δ 70.4 (C-15), and the key COSY correlations (Fig. 3) of δ 4.28, m (H-15) with δ 1.02, m (H-14), and δ 2.57, ddd; 1.63, overlap (H_2-16). OH at C-15 was determined as β *via* the key NOESY correlations (Fig. 4) of α-oriented H-15 (δ 4.28, m) with *axially*-oriented H-14 (δ 1.02, m), and H-17 (δ 3.57, overlap). The structure of **14** was thus determined as 7β,15β-dihydroxy metenolone.

Compounds **1**–**14** were evaluated for inhibition of T-cell proliferation, and cytokine (TNF-α) production in cell-based assays. Compounds **1** (62.5 ± 4.4%), **2** (73.4 ± 0.6%), **5** (81.0 ± 2.5%), **8** (69.7 ± 1.4%), **10** (73.2 ± 0.3%), **11** (60.1 ± 3.3%), and **12** (71.0 ± 7.2%) showed a good inhibition of cytokine (TNF-α) production. Compounds **3** (53.7 ± 1.4%), **7** (46.6 ± 5.2%), and **14** (52.9 ± 2.4%) showed a moderate activity, compounds **4** (33.5 ± 6.6%), and **6** (37.8 ± 1.1%) showed a weak activity, while metabolites **9**, and **13** were found as inactive. Compounds **3** (IC_{50} = 4.4 ± 0.01 μg/mL), and **5** (IC_{50} = 10.2 ± 0.01 μg/mL) showed a significant activity against T-cells proliferation, in comparison to standard drug, prednisolone (IC_{50} = 3.51 ± 0.03 μg/mL). Metabolite **8** (IC_{50} = 21.1 ± 0.04 μg/mL) showed a moderate activity, while compound **2** (IC_{50} = 68.9 ± 0.02 μg/mL) showed a weak activity against T-cell proliferation. Compounds **1**, **4**, **6**, **7**, and **9**–**14** were identified as inactive against T-cell proliferation.

Structure-activity relationships (SARs)

Apparently, dihydroxylation of metenolone acetate (**1**) (hydroxylation at C-15, and C-20) has increased the inhibition potential of compound **5** (81.0 ± 2.5%) against TNF-α production, in comparison to the substrate **1** (62.5 ± 4.4%). Similarly, an OH group at C-6 in metabolite **2** (73.4 ± 0.6%) also increased its inhibition potential against TNF-α production. Hydrolysis of ester moiety in compound **8** (69.7 ± 1.4%) has enhanced its activity against TNF-α production. Oxidative cleavage at C-17, and β-H at C-5 in metabolite **10** (73.2 ± 0.3%) has also enhanced its anti-inflammatory activity. Metabolite **12** (atamestane) (71.0 ± 7.2%) with oxidative cleavage of ester moiety at C-17, and dehydrogenation between C-4/C-5 also showed a good inhibition of TNF-α production, in comparison to the drug **1**. Hydrolysis at C-17, oxidation at C-12, and dehydrogenation at C-5/C-4 as in metabolite **11** (60.1 ± 3.3%) showed a similar inhibition potential against TNF-α production, as compared to the metenolone acetate (**1**).

Conclusion

In the present research, metenolone acetate (**1**), an anabolic drug, was structurally modified by using *R. stolonifer*, *A. alliaceous*, *F. lini*, and *C. elegans*, where seven new and six known derivatives of **1** were obtained. Atamestane (**12**), an aromatase inhibitor, was synthesized for the first time through *F. lini*-mediated transformation of **1**. During bio-catalysis, oxidation, dehydrogenation, and reduction were mainly occurred. The study indicated that *F. lini* was able to catalyze dehydrogenation reactions selectively. Compounds **1**–**14** were identified as non-cytotoxic against BJ (normal human fibroblast) cell line. Metabolites **5** (81.0 ± 2.5%), **2** (73.4 ± 0.6%), **8** (69.7 ± 1.4%), **10** (73.2 ± 0.3%), **11** (60.1 ± 3.3%), and **12** (71.0 ± 7.2%) showed a potent activity against TNF-α production, in comparison to the **1** (62.5 ± 4.4%). In future, metabolites **2**–**14** will be studied at enzymatic level by using different techniques in order to understand the mechanisms involved in the biocatalytic structural modification reactions. These findings thus form the basis for further research towards drug discovery against chronic inflammatory diseases.

Compliance with Ethics Requirements

This article does not contain any studies with human or animal subjects.

Declaration of Competing Interest

The authors declare that they have no known competing financial interests or personal relationships that could have appeared to influence the work reported in this paper.

Acknowledgements

Authors acknowledge the enabling role of the Searle Company Ltd. Pakistan, through research funding, and also financial support of Higher Education Commission, Pakistan, through research project # 7993.

References

[1] Maltais R, Tremblay MR, Ciobanu LC, Poirier D. Steroids and combinatorial chemistry. J Comb Chem 2004;6(4):443–56.
[2] Shahidi NT. A review of the chemistry, biological action, and clinical applications of anabolic-androgenic steroids. Clin Ther 2001;23(9):1355–90.
[3] Fernandes P, Cruz A, Angelova B, Pinheiro HM, Cabral JMS. Microbial conversion of steroid compounds: recent developments. Enzyme Microb Technol 2003;32(6):688–705.
[4] Maravelias C, Dona A, Stefanidou M, Spiliopoulou C. Adverse effects of anabolic steroids in athletes: a constant threat. Toxicol Lett 2005;158(3):167–75.
[5] Ho EN, Leung DK, Wan TS, Nola HY. Metabolic studies of methenolone acetate in horses. Anal Chim Acta 2005;540(1):111–9.
[6] Goudreault D, Massé R. Studies on anabolic steroids-4. Identification of new urinary metabolites of methenolone acetate (primobolan®) in human by gas chromatography/mass spectrometry. J Steroid Biochem Mol Biol 1990;37(1):137–54.
[7] Fragkaki AG, Angelis YS, Kiousi P, Georgakopoulos CG, Lyris E. Comparison of sulfo-conjugated and gluco-conjugated urinary metabolites for detection of methenolone misuse in doping control by LC-HRMS, GC-MS and GC-HRMS. J Mass Spectrom 2015;50(5):740–8.
[8] Hussain Z, Dastagir N, Hussain S, Jabeen A, Zafar S, Malik R, et al. *Aspergillus niger*-mediated biotransformation of methenolone enanthate, and immunomodulatory activity of its transformed products. Steroids 2016;112:68–73.
[9] Bianchini LF, Arruda MF, Vieira SR, Campelo P, Grégio AM, Rosa EA. Microbial biotransformation to obtain new antifungals. Front Microbiol 2015;6:1433.
[10] Alcántara AR. Biotransformations in drug synthesis: a green and powerful tool for medicinal chemistry. J Med Chem Drug Des 2017;1:1–7.
[11] Hegazy MEF, Mohamed TA, ElShamy AI, Abou-El-Hamd HM, Mahalel UA, Reda EH, et al. Microbial biotransformation as a tool for drug development based on natural products from mevalonic acid pathway: a review. J Adv Res 2015;6(1):17–33.
[12] Schulz S, Girhard M, Urlacher VB. Biocatalysis: key to selective oxidations. ChemCatChem 2012;4(12):1889–95.
[13] Sheldon RA. The E factor: fifteen years on. Green Chem 2007;9(12):1273–83.
[14] Sheldon RA. E factors, green chemistry and catalysis: an odyssey. Chem Commun 2008;29:3352–65.
[15] Sheldon RA, Woodley JM. Role of biocatalysis in sustainable chemistry. Chem Rev 2017;118:801–38.
[16] Urlacher VB, Girhard M. Cytochrome P450 monooxygenases: an update on perspectives for synthetic application. Trends Biotechnol 2012;30(1):26–36.

[17] Coussens LM, Werb Z. Inflammation and cancer. Nature 2002;420 (6917):860–7.
[18] Balkwill F, Mantovani A. Inflammation and cancer: back to Virchow?. The Lancet 2001;357(9255):539–45.
[19] Chapman KE, Coutinho AE, Zhang Z, Kipari T, Savill JS, Seckl JR. Changing glucocorticoid action: 11β-hydroxysteroid dehydrogenase type 1 in acute and chronic inflammation. J Steroid Biochem Mol Biol 2013;137:82–92.
[20] Atia-tul-Wahab SM, Ibrahim I, Hussain A, Ajandouz EH, Hijazi A, et al. *Cunninghamella blakesleeana*-mediated biotransformation of a contraceptive drug, desogestrel, and anti-MDR-*Staphylococcus aureus* activity of its metabolites. Bioorg Chem 2018;77:52–158.
[21] Siddiqui M, Atia-tul-Wahab Ahmad MS, Yousuf S, Fatima N, Shaikh NN, et al. Biotransformation of a potent anabolic steroid, mibolerone, with *Cunninghamella blakesleeana*, *C. echinulata*, and *Macrophomina phaseolina*, and biological activity evaluation of its metabolites. PLoS ONE 2017;12(2): e0171476.
[22] Baydoun E, Karam M, Atia-tul-Wahab, Khan MSA, Ahmad MS, Smith C, et al. Microbial transformation of nandrolone with *Cunninghamella echinulata* and *Cunninghamella blakesleeana* and evaluation of leishmanicidal activity of transformed products. Steroids 2014;2014(88):95–100.
[23] Choudhary MI, Siddiqui M, Atia-tul-Wahab, Yousuf S, Fatima N, Ahmad MS, et al. Bio-catalytic structural transformation of anti-cancer steroid, drostanolone enanthate with *Cephalosporium aphidicola* and *Fusarium lini*, and cytotoxic potential evaluation of its metabolites against certain cancer cell lines. Front Pharmacol 2017;8:900.
[24] Bano S, Atia-tul-Wahab, Yousuf S, Jabeen A, Mesaik MA, Choudhary MI. New anti-inflammatory metabolites by microbial transformation of medrysone. Plos One 2016;11(4):e0153951.
[25] Farooq R, Hussain N, Yousuf S, Atia-tul-Wahab, Ahmad MS, Atta-ur-Rahman, et al. Microbial transformation of mestanolone by *Macrophomina phaseolina* and *Cunninghamella blakesleeana* and anticancer activities of the transformed products. RSC Adv 2018;8(39):21985–92.
[26] Ahmad MS, Zafar S, Yousuf S, Atta-ur-Rahman, Atia-tul-Wahab, Choudhary MI. Biotransformation of 6-dehydroprogesterone with *Aspergillus niger* and *Gibberella fujikuroi*. Steroids 2016;112:62–7.
[27] Ahmad MS, Zafar S, Bibi M, Bano S, Atta-ur-Rahman, Atia-tul-Wahab, Choudhary MI. Biotransformation of androgenic steroid mesterolone with *Cunninghamella blakesleeana* and *Macrophomina phaseolina*. Steroids 2014;82:53–9.
[28] Choudhary MI, Sultan S, Jalil S, Anjum S, Rahman AA, Fun HK, et al. Microbial transformation of mesterolone. Chem Biodivers 2005;2(3):392–400.
[29] Baydoun E, Bano S, Atia-tul-Wahab, Jabeen A, Yousuf S, Mesaik A, et al. Fungal transformation and T-cell proliferation inhibitory activity of melengestrol acetate and its metabolite. Steroids 2014;86:56–61.
[30] Helfand SL, Werkmeister J, Roder JC. Chemiluminescence response of human natural killer cells. I. The relationship between target cell binding, chemiluminescence, and cytolysis. J Exp Med 1982;156(2):492–505.
[31] Ahmed SA, Gogal Jr RM, Walsh JE. A new rapid and simple non-radioactive assay to monitor and determine the proliferation of lymphocytes: an alternative to [3H] thymidine incorporation assay. J Immunol Methods 1994;170(2):211–24.
[32] Lourdusamy M, Labrie F, Singh SM. Synthesis of Atamestane (SH 489): an Aromatase Inhibitor. Synthetic Commun 1995;25(22):3655–62.
[33] Kuhnz W, Hoyer GA, Backhus S, Jakobs U. Metabolism of the steroidal aromatase inhibitor atamestane in rats, cynomolgus monkeys and humans. Eur J Drug Metab Ph 1994;19(2):137–50.